JOC The Journal of Organic Chemistry

Article

pubs.acs.org/joc

Tuning Emission Responses of a Triphenylamine Derivative in Host–Guest Complexes and an Unusual Dynamic Inclusion Phenomenon

Monalisa Gangopadhyay,[†] Amal K. Mandal,[§] Arunava Maity,[†] Sapna Ravindranathan,[‡] Pattuparambil R. Rajamohanan,*[,‡] and Amitava Das*[,†]

[†]Organic Chemistry Division and [‡]Central NMR Facility, CSIR-National Chemical Laboratory, Pune, Maharashtra 411008, India

[§]Molecular Nanofabrication, University of Twente, Hallenweg 15, 7522 Enschede, The Netherlands

Supporting Information

ABSTRACT: A newly synthesized triphenylamine derivative ($\mathbf{1}Cl_3$) shows significant differences in inclusion complex formation with two different macrocyclic hosts, cucurbit[7]uril (CB[7]) and β-cyclodextrin (β-CD). Detailed investigations by NMR spectroscopy reveal that CB[7] forms a 1:3 host–guest complex ($[\mathbf{1}\cdot 3\{CB[7]\}]Cl_3$) in which three arms of $\mathbf{1}Cl_3$ are bound to three host molecules. On the other hand, β-CD forms a dynamic 1:1 inclusion complex ($[\mathbf{1}\cdot\{\beta\text{-CD}\}]Cl_3$) by binding to only one of the three arms of $\mathbf{1}Cl_3$ at a given time. The formation of a 1:1 host–guest complex with β-CD and 1:3 host–guest complex with CB[7] was also confirmed from the results of the isothermal titration calorimetric studies. Interestingly, $\mathbf{1}Cl_3$ exhibits a rare dual emission property in solution at room temperature with the lower and higher energy bands arising from a locally excited state and an intramolecular charge-transfer transition, respectively. The difference in inclusion complex formation behavior of $\mathbf{1}Cl_3$ with the two macrocyclic hosts results in the stabilization of different emission states in the two inclusion complexes. The fundamental difference in the electrostatic surface potentials, cavity polarities, and shapes of the two macrocyclic hosts could account for the formation of the different inclusion complexes with distinct luminescence responses.

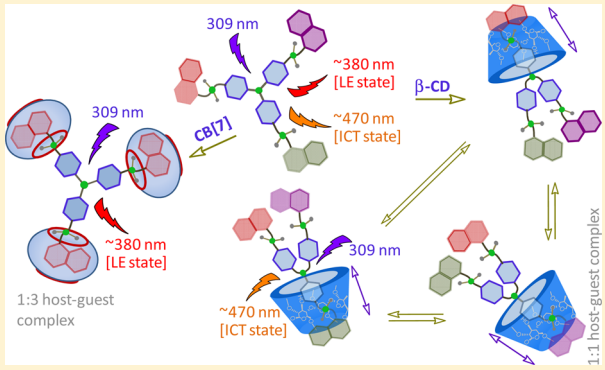

INTRODUCTION

In recent years considerable attention has been focused on understanding and controlling the electroluminescence phenomenon in triphenyl amine (TPA) derivatives since they are expected to be significant in various technological applications.[1−3] In most of these applications, molecular rigidity of TPA derivatives plays a major role.[4] Previous reports on structural and theoretical aspects of various TPA derivatives suggest that these molecules preferentially adopt a three-bladed propeller structure with some degree of conformational flexibility, which adversely influences their photoluminescence properties and, thus, their application potential.[5,6] Significant efforts have been directed toward controlling the conformational flexibility of TPA derivatives, mostly by intricate synthesis of highly rigid frameworks.[7] More recently, attempts have been made to utilize host–guest inclusion complex formation with different macrocyclic hosts like cyclodextrin (CD), cucurbit[7]uril (CB[7]), etc. However, such examples are scarce in the literature. Also, dual emission behavior has remained elusive for all TPA derivatives reported to date. Dual emission from a single molecule at room temperature, following excitation at a single wavelength, has special significance in biomedical imaging, multiplex signaling, dual labeling, optoelectronics, and display devices.[8−12] Dual emission is not an uncommon phenomenon either at low temperature or in rigid media; however, it is rather unique in the solution state at room temperature.[13] Several strategies have been adopted by chemists and material scientists for developing appropriate materials capable of exhibiting dual emission behavior, including the use of quantum dots (QDs) with various size distributions and a few heteroleptic Ru(II)–polypyridyl complexes with decoupled excited states.[14,15] Dual emission at room temperature has also been achieved in molecular conjugates having two or more fluorophores covalently bound to a protein backbone.[16] However, these approaches have their own limitations which usually involve elaborate procedures/methodologies, and such reports are not common in contemporary literature.[17] Some recent reports have also shown that supramolecular self-assembly and/or integrative self-sorting phenomena could be used judiciously for achieving complex molecular architectures and tunable optical properties.[4,18−21] In this article, we report the synthesis of a unique TPA derivative, $\mathbf{1}Cl_3$ (Figure 1) with two decoupled excited states which show dual emission behavior in solution at room temperature. For example, in dimethylformamide (DMF) solution, $\mathbf{1}Cl_3$ exhibits a high-energy excitation band at ∼370 nm for a locally excited (LE) state and a low-energy band for

Received: October 11, 2015
Published: December 9, 2015

DOI: 10.1021/acs.joc.5b02353
J. Org. Chem. 2016, 81, 512−521

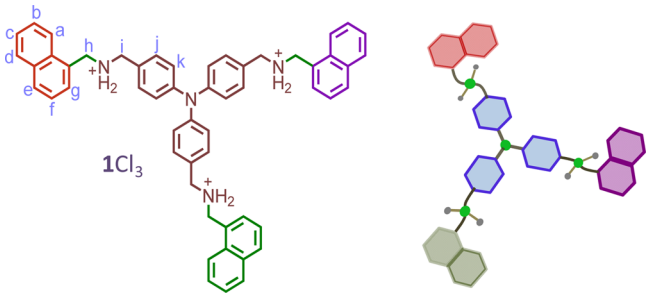

Figure 1. Schematic representation of the guest molecule $\mathbf{1}Cl_3$.

the intramolecular charge-transfer (ICT) process at ~440 nm. Formation of inclusion complexes with CB[7] and *β*-CD imparts conformational rigidity to $\mathbf{1}Cl_3$ allowing tuning of the dual emission behavior.

NMR investigations along with steady-state and time-resolved emission studies reveal that complexation of $\mathbf{1}Cl_3$ with CB[7] results in the formation of a 1:3 host–guest complex ($[\mathbf{1}\cdot\{3CB[7]\}]Cl_3$) in which the LE state is preferentially stabilized. On the other hand, a dynamic 1:1 host–guest complex ($[\mathbf{1}\cdot\{\beta\text{-CD}\}]Cl_3$) is formed with *β*-CD, with a preference for the ICT-based luminescence state. We rationalize the formation of the two distinctly different inclusion complexes with markedly dissimilar luminescence responses on the basis of the different shapes of the host molecules and the significant differences in their electrostatic surface potentials and cavity polarities.

RESULTS AND DISCUSSION

The TPA derivative, $\mathbf{1}Cl_3$, was synthesized by reacting naphthalen-1-ylmethanamine with tris(4-formylphenyl)amine as described in the Experimental Section and was characterized using various analytical and spectroscopic techniques (Figure S1 Supporting Information). The inclusion complex formation of $\mathbf{1}Cl_3$ with CB[7] and *β*-CD was examined in detail by employing NMR spectroscopy, and the thermodynamics of the binding process was studied by ITC measurements. The luminescence properties of the TPA fragment in the free state and in the inclusion complexes were investigated by steady-state and time-resolved emission studies.

NMR Studies of $[\mathbf{1}\cdot\{3CB[7]\}]Cl_3$. ^{1}H NMR spectra of $\mathbf{1}Cl_3$, CB[7], and the inclusion complex, $[\mathbf{1}\cdot\{3CB[7]\}]Cl_3$ formed by the addition of 4 mol equiv of CB[7] to $\mathbf{1}Cl_3$ are shown in Figure 2. Titration studies showed broad NMR signals for $\mathbf{1}Cl_3$ at $\mathbf{1}Cl_3$:CB[7] ratio of 1:1, but line narrowing was observed with further addition of CB[7] (Figure S2, Supporting Information). No significant changes were observed in the NMR spectrum recorded at a molar ratio of 1:3 and above. This suggests that at lower concentrations of CB[7], $\mathbf{1}Cl_3$ exchanges between the free and bound forms (inclusion complex), but at molar ratios of 1:3 and above, a stable inclusion complex is formed. At a molar ratio of 1:3 for $\mathbf{1}Cl_3$:CB[7], an inclusion complex is formed in which each of the three arms of $\mathbf{1}Cl_3$ are bound to a host molecule (CB[7]). At molar ratios exceeding 1:3, all guest molecules are bound, however the proton signals of CB[7] splits into two sets corresponding to bound and free forms of the host, with the former being more shielded and showing characteristic exchange broadened lines (Figure S3, Supporting Information).

Chemical shift assignments in $[\mathbf{1}\cdot\{3CB[7]\}]Cl_3$ were obtained by 1D and 2D NMR experiments (Figures S4–S6, Supporting Information). Chemical shift changes in $\mathbf{1}Cl_3$ and CB[7] on complex formation are evident in Figure 2. In $\mathbf{1}Cl_3$, all protons of the naphthyl moieties show upfield shifts ($\Delta\delta_{H_a}$ = −0.33, $\Delta\delta_{H_c}$ = −0.34, $\Delta\delta_{H_d}$ = −0.52, $\Delta\delta_{H_e}$ = −0.76, $\Delta\delta_{H_f}$ = −0.60, and $\Delta\delta_{H_g}$ = −0.35 ppm), while protons H_j and H_k of the phenyl moiety show downfield shifts ($\Delta\delta_{H_j}$ = 0.36 ppm and $\Delta\delta_{H_k}$ = 0.21 ppm). In addition, the aliphatic proton H_i shows a significant downfield shift ($\Delta\delta_{H_i}$ = 0.41 ppm) whereas the H_h proton experiences a marginal upfield shift ($\Delta\delta_{H_h}$ = −0.07 ppm). In CB[7], the diastereotopic protons (H_1, H_2) of the methylene linkers, which appear at 5.75 and 4.18 ppm as two doublets, shift to 5.67 and 4.13 ppm on complex formation. Due to symmetry, all the 14 methylene linkers of each of the two rims of CB[7] are equivalent in free CB[7] as well as in the complex. The methine protons (H_3) of CB[7] shifts from 5.47 to 5.37 ppm on complex formation. In inclusion complexes with CB[7], protons of guest molecules experience a relatively shielded environment within the CB[7] cavity compared to the uncomplexed state.[22] The observed upfield shifts of the

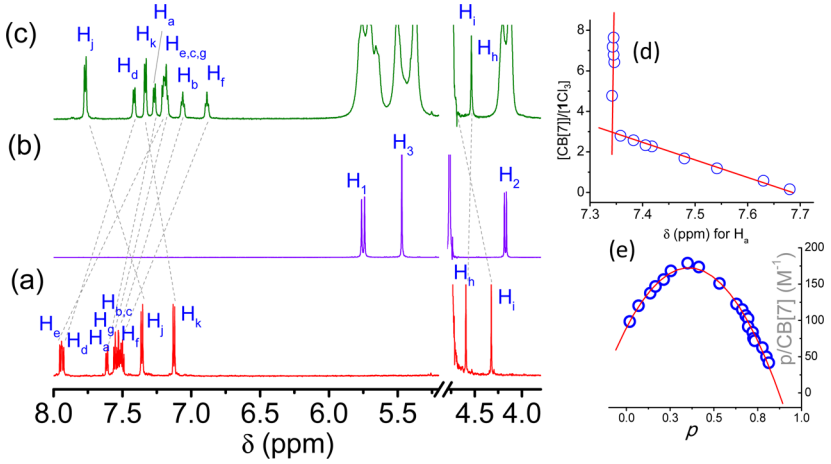

Figure 2. (a) Partial ^{1}H NMR spectra of 3.73×10^{-3} M aqueous solution of $\mathbf{1}Cl_3$, (b) 3.73×10^{-3} M aqueous solution of CB[7], (c) the inclusion complex with $\mathbf{1}Cl_3$:CB[7] mole ratio 1:4, (d) mole ratio plot for the complexation of $\mathbf{1}Cl_3$ with CB[7] using $\Delta\delta$ for the H_a proton in $\mathbf{1}Cl_3$ and (e) Scatchard plot for the inclusion complex formation. The data are fit by the curve $y = 89.87 + 462.84x - 648.91x^2$ (r^2 = 0.97).

DOI: 10.1021/acs.joc.5b02353
J. Org. Chem. 2016, 81, 512–521

naphthyl protons in [**1**·{3CB[7]}]Cl_3 imply that only the naphthyl moieties from each arm of **1**Cl_3 are located within the CB[7] cavity on complex formation.

Binding stoichiometry for the host–guest complex formation between **1**Cl_3 and CB[7] was evaluated based on the data obtained from NMR titration studies. The mole ratio plot generated by monitoring the chemical shift change of the H_a proton of **1**Cl_3 shows no further changes in chemical shift on addition of more than three equivalents of CB[7] (Figure 2d). This indicates a 1:3 binding stoichiometry and the formation of a 1:3 host–guest complex ([**1**·3{CB[7]}]Cl_3). This was further substantiated by MALDI-TOF mass spectral studies, which showed a molecular ion peak corresponding to [**1**·3{CB[7]}]-Cl_3 (Figure S7, Supporting Information). The Scatchard plot[22] was generated based on the extent of complexation *p*, estimated from the Benesi–Hildebrand (B–H) plot (Figure S8, Supporting Information). The nonlinear nature of the Scatchard plot with a maximum confirms that positive cooperativity drives the complex formation process (Figure 2e). The initial formation of a 1:1 host–guest complex in which one arm of **1**Cl_3 is bound to CB[7] favors the sequential binding of the second and third host molecules to the remaining arms of **1**Cl_3, eventually resulting in a 1:3 host–guest complex. Limited solubility of the host–guest complex ([**1**·3{CB[7]}]Cl_3) at the concentration level that was used for NMR studies did not allow the precise evaluation of the individual binding constant for 1:3 complex formation or the composite binding constant by NMR spectroscopy.

Further insights into the nature of the intermolecular interactions in the host–guest complex were obtained by 2D NMR experiments (NOESY and ROESY). These experiments were carried out on samples with **1**Cl_3:CB[7] ratios of 1:3 or more to ensure conditions under which a 1:3 inclusion complex is formed. The NOESY and ROESY spectra (Figure 3 and

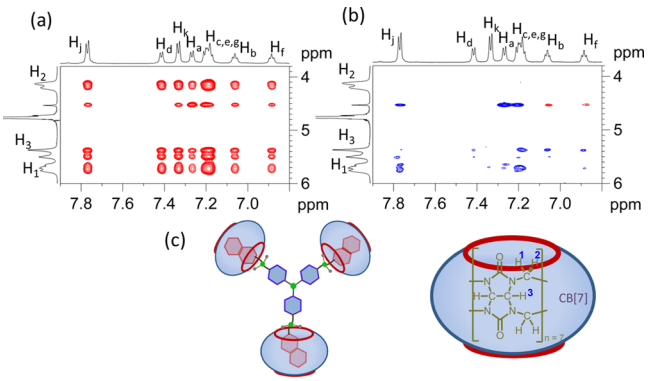

Figure 3. 2D NMR spectra showing intermolecular cross peaks in the [**1**·3{CB[7]}]Cl_3 complex (a) NOESY and (b) ROESY. (c) Schematic representation of the 1:3 host–guest complex.

Figure S9, Supporting Information) show strong intra- and intermolecular cross peaks. The positive cross peaks observed in the NOESY spectrum indicate a slowing down of the overall motion on complex formation resulting in a rotational correlation time which falls in the long correlation limit ($\omega_0\tau_c \gg 1$). Intermolecular cross peaks in the NOESY spectrum can arise from the spatial proximity of the host and guest as a result of complex formation or due to exchange and spin diffusion effects. The ROESY spectrum helps to distinguish cross peaks arising due to spatial proximity (negative cross peaks) from those arising as a result of exchange (positive cross peaks). Among two inequivalent methylene protons of CB[7], those at 5.67 ppm (H_1) show intermolecular cross peaks to the naphthyl protons (H_c and H_e) located within the CB[7] cavity as well as the phenyl proton H_j located outside the cavity (Figure 3). On the other hand, intermolecular cross peaks to the methylene linker proton of CB[7] at 4.13 ppm are observed only in the NOESY spectrum but not in the ROESY spectrum. This implies that this cross peak in the NOESY spectrum arises from spin diffusion effects at the long mixing time (1s) employed. The structure of CB[7] shows that the inequivalent methylene linker protons at 5.67 and 4.13 ppm are present on both rims of CB[7], however the linker protons of the two rims are indistinguishable in the spectrum due to the degeneracy of the chemical shifts imposed by symmetry. The observation of cross peaks from the methylene protons of CB[7] at 5.67 ppm to both naphthyl and phenyl units of **1**Cl_3 indicates the spatial proximity of the linker protons to both these units of the guest molecule. This is because the linker protons at both rims contribute to the signal at 5.67 ppm. Thus, cross peaks to the naphthyl protons arise due to spatial proximity to the linker protons at one of the rims, while the phenyl protons show cross peaks to the equivalent linker protons at the opposite rim. The ROESY spectrum also shows intermolecular cross peaks between the methine protons of CB[7] at 5.37 ppm and the naphthyl protons H_c, H_e, H_b, and H_f, the latter two being weaker. Based on these observations and the chemical shift changes induced in the proton spectrum on complex formation, we envisage the formation of a 1:3 inclusion complex as shown in Figure 3c. All the additional cross peaks seen in the NOESY spectrum, which are absent in the ROESY spectrum, are exchange cross peaks between free and bound forms of CB[7] since the sample had a **1**Cl_3:CB[7] mole ratio slightly in excess of 1:3.

NMR Studies of [1·{*β*-CD}]Cl_3. ^{1}H NMR spectra of **1**Cl_3 and the inclusion complex formed by the addition of 4 mol equiv of *β*-CD are shown in Figure 4. As in the case of CB[7],

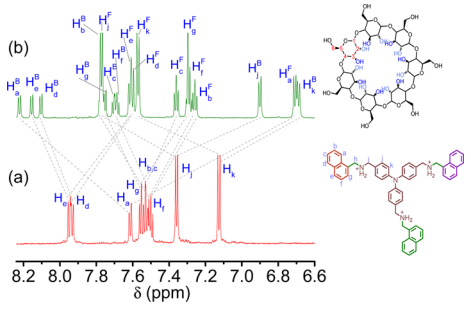

Figure 4. Partial ^{1}H NMR spectra of (a) 1.64×10^{-3} M aqueous solution of **1**Cl_3 and (b) inclusion complex, with **1**Cl_3:*β*-CD mole ratio of 1:4. Signals from the "bound" and "free" arms of **1**Cl_3 in the complex are labeled "B' and 'F", respectively. The structures of **1**Cl_3 and *β*-CD with labeling of atoms are also indicated.

host–guest complex formation results in both shielding and deshielding influences on the aromatic protons of **1**Cl_3. Titration studies with *β*-CD and CB[7] show striking differences in the changes occurring in the **1**Cl_3 spectra as host concentration increases (Figures S2 and S10, Supporting Information).

Unlike observations for the complex with CB[7], the chemical shifts of **1**Cl_3 protons remain almost unchanged on addition of 1.0, 2.0, 3.0, and 6.0 mol equiv of *β*-CD. Also, in

DOI: 10.1021/acs.joc.5b02353
J. Org. Chem. 2016, 81, 512–521

contrast to complex formation with CB[7], more signals are observed in the spectrum of the complex with β-CD. This is readily visible in the homodecoupled pure shift NMR spectra shown in Figure 5, recorded using the PSYCHE method.[24] The

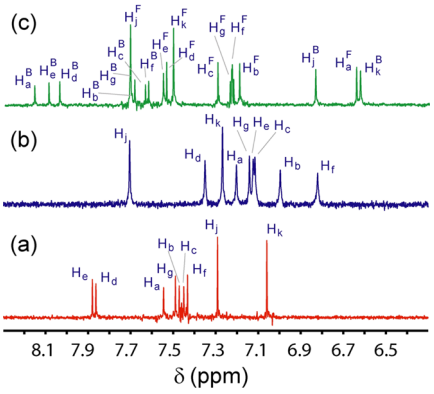

Figure 5. Comparison of the 700 MHz pure shift ^{1}H NMR spectra of the aromatic region at 298 K for (a) $\mathbf{1}Cl_3$ and inclusion complex of $\mathbf{1}Cl_3$ (b) with CB[7] at mole ratio 1:4 and (c) with β-CD at mole ratio 1:4.

spectrum of the inclusion complex formed between $\mathbf{1}Cl_3$ and CB[7] shows nine different types of $\mathbf{1}Cl_3$ protons, while the spectrum of the complex formed between $\mathbf{1}Cl_3$ and β-CD shows as many as 18 proton environments. The presence of well-defined sharp signals implies that the additional signals could be due to the presence of bound and free $\mathbf{1}Cl_3$ which may be in slow exchange or due to the inequivalence of the three arms in the complex formed between $\mathbf{1}Cl_3$ and β-CD. However, titration studies do not show any signals of free $\mathbf{1}Cl_3$ at $\mathbf{1}Cl_3$:β-CD ratios exceeding 1:1 (Figure S10, Supporting Information) indicating that the presence of free $\mathbf{1}Cl_3$ cannot account for the additional signals in the spectrum.

In order to obtain the chemical shift assignments and explain the presence of additional signals of $\mathbf{1}Cl_3$ in the complex with β-CD, detailed 1D and 2D NMR investigations were carried out (Figures S11–S17, Supporting Information). These studies indicate that the signals of $\mathbf{1}Cl_3$ in the host–guest complex are doubled in number and occur with a ratio of 1:2. This suggests that one of the arms of $\mathbf{1}Cl_3$ behaves differently from the other two in the complex. Such a possibility can arise if only one of the three arms of $\mathbf{1}Cl_3$ is bound during complex formation with β-CD. For example, the spectra in Figure 4 show that the H_j and H_k protons of the triphenylamine groups give rise to two sets of signals in the complex with a ratio of 1:2. The signals with higher intensity are deshielded (H_j = 7.53 ppm, H_k = 7.74 ppm), while the lower intensity signals are shielded (H_j = 6.87 ppm, H_k = 6.68 ppm) with respect to those of neat $\mathbf{1}Cl_3$ (H_j = 7.35 ppm, H_k = 7.11 ppm). The observed intensity ratios suggest that the deshielded protons belong to the "free" arms of $\mathbf{1}Cl_3$ and the shielded proton belongs to the arm "bound" to β-CD. Similar behavior is observed for the methylene protons (H_h and H_i) of $\mathbf{1}Cl_3$ on complex formation (Figure S18, Supporting Information). For $\mathbf{1}Cl_3$, H_i and H_h protons appear as singlets at ∼4.3 and ∼4.6 ppm, respectively. On formation of the host–guest complex, signals of the H_h protons of the "free" arms are shielded (singlet at 4.09 ppm), whereas the H_h proton of the "bound" arm is deshielded and appears as an AB quartet (4.73 and 4.83 ppm, J = 13.7 Hz). Similarly, the H_i proton of the "bound" arm experiences deshielding and occurs as an AB quartet (4.34 and 4.31 ppm, J = 13.4 Hz), while those of the "free" arms show a deshielded AB quartet (4.01 and 3.85 ppm, J = 13.2 Hz).

Another striking feature of the ^{1}H NMR spectrum is the presence of a heavily shielded doublet at 6.71 ppm, assigned to the H_a proton of the naphthyl moiety (Figure 4). The chemical shift difference of H_a with respect to neat $\mathbf{1}Cl_3$ is ∼0.9 ppm. The integrated peak area suggests that it originates from the two "free" arms of $\mathbf{1}Cl_3$. Interestingly, the H_a proton of the "bound" arm of $\mathbf{1}Cl_3$ is considerably deshielded due to its interaction with the smaller rim of β-CD and appears as a doublet at 8.19 ppm which is shifted by ∼0.42 ppm with respect to neat $\mathbf{1}Cl_3$. Upfield shift of aromatic protons on inclusion in the β-CD cavity is not uncommon. However, the appreciable upfield shift of ∼0.9 ppm for the two naphthyl H_a protons of the "free" arms of $\mathbf{1}Cl_3$ on host–guest complex formation with β-CD is rather unusual. The observed shielding of the H_a protons of the two "free" arms can only be explained by considering an efficient π–π stacking interaction involving the naphthyl rings of the "free" arms. This is possible if the two "free" arms approach sufficiently close to each other to experience a π–π stacking interaction as indicated in Scheme 1. Influence of π–π stacking interaction in dictating the

Scheme 1. Cartoon Representation of the 1:1 Host–Guest Complex ($[\mathbf{1}\cdot\{\beta\text{-CD}\}]Cl_3$) Formed Between $\mathbf{1}Cl_3$ and β-CD Molecule, Where Only One Arm of $\mathbf{1}Cl_3$ Is Bound at a Time[a]

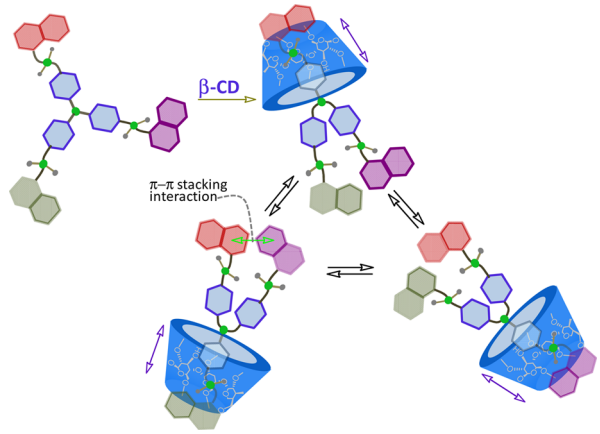

[a]The equivalence of the three arms results in a dynamic inclusion complex in which one β-CD molecule may bind to any one of the three arms. The exchange equilibrium is indicated by using different colors for the naphthyl groups of the three arms.

conformation in a host–guest complex has been reported.[23b] Even though most of the naphthyl protons of the "free" arms of $\mathbf{1}Cl_3$ show upfield shifts and corresponding downfield shifts for the "bound" arm, the magnitude of these shifts is less when compared to that seen for the H_a protons of the "free" arms (Figure 4). These observations further corroborate the formation of a 1:1 host–guest complex ($[\mathbf{1}\cdot\{\beta\text{-CD}\}]Cl_3$), in which the naphthyl moieties of the two unbound arms of $\mathbf{1}Cl_3$ approach close enough to induce a π–π stack interaction as shown in Scheme 1.

Variable-temperature ^{1}H NMR spectra of $[\mathbf{1}\cdot\{\beta\text{-CD}\}]Cl_3$ provide further evidence for the stacking interaction (Figure S19, Supporting Information). The shielded H_a protons show substantial downfield shifts as the temperature increases.

DOI: 10.1021/acs.joc.5b02353
J. Org. Chem. 2016, 81, 512–521

Enhanced molecular flexibility at higher temperatures is expected to reduce the possibility of $\pi-\pi$ stack interactions thereby decreasing the shielding influence on the H_a proton. In contrast, the H_k protons of the phenyl moiety of the "free" arms, which are not under the influence of $\pi-\pi$ stack interaction, show only a marginal upfield shift as temperature increases. Similar effects of the influence of temperature on the $\pi-\pi$ stacking interaction are also seen for the H_h and H_i protons of the "free" arms (Figure S20, Supporting Information). The proton resonances of the host β-CD are also split into two sets of unequal intensity providing further evidence for the formation of a 1:1 host–guest complex. The weaker signals arising from β-CD bound to $\mathbf{1}Cl_3$ are shielded, while the stronger signals are unaffected compared to the ^1H NMR signals of unbound β-CD (Figure S18, Supporting Information). Interestingly, the ratio of the area of a single aromatic proton of the "bound" arm of $\mathbf{1}Cl_3$ to one of the weaker signals of β-CD, (for example, H_a of the "bound" arm at 8.19 to H_1 of bound β-CD at ~4.9 ppm) is 1:7. Since one molecule of β-CD has seven equivalent H_1 protons, the ratio of 1:7 is consistent with the formation of a 1:1 host–guest complex in which only one arm of $\mathbf{1}Cl_3$ resides in the β-CD cavity. The results of ESI-MS studies (Figure S21, Supporting Information) and the mole ratio plot analysis (Figure S22, Supporting Information) also support the formation of the proposed 1:1 host–guest complex ($[\mathbf{1}\cdot\{\beta\text{-CD}\}]Cl_3$) depicted in Scheme 1.

The dynamic nature of the $[\mathbf{1}\cdot\{\beta\text{-CD}\}]Cl_3$ complex is evident from the changes in the line widths of the $\mathbf{1}Cl_3$ signals in the variable-temperature ^1H NMR spectra (Figures S19 and S20, Supporting Information). The sharp signals observed at 298 K broaden at temperatures above 323 K, which implies that the exchange process shifts from slow to intermediate NMR time scales as temperature increases. The exchange between complexed and free $\mathbf{1}Cl_3$ seems unlikely since the spectra do not show signals corresponding to free $\mathbf{1}Cl_3$ in the presence of one or more mole equivalents of β-CD.

In order to obtain further insights into the exchange process, we carried out NOESY experiments with a solution having $\mathbf{1}Cl_3$:β-CD molar ratio of 1:4. The NOESY spectra show strong positive intermolecular cross peaks indicating complex formation (Figure S15 and S16, Supporting Information). Interestingly, the protons of the "free" and "bound" arms of $\mathbf{1}Cl_3$ show cross peaks between them (for example, H_a^F at 6.71 to H_a^B at 8.19) and also to the protons of β-CD (Figure S16, Supporting Information). The cross peaks between the "bound" and "free" arms of $\mathbf{1}Cl_3$ imply an exchange equilibrium between them, mediated by β-CD molecules in solution. A single arm of $\mathbf{1}Cl_3$ in the 1:1 host–guest complex is bound to a β-CD molecule at a given time. Since the three arms are equivalent, it is equally probable that another β-CD molecule from the bulk could bind to one of the two "free" arms while releasing the arm which was initially bound.

The nature of the exchange process was further substantiated by ROESY experiments (Figure 6 and Figure S17, Supporting Information), which showed two types of cross peaks: those arising from spatial proximity (negative cross peaks) and those due to chemical exchange (positive cross peaks).

The positive exchange cross peaks between the "bound" and "free" arms of $\mathbf{1}Cl_3$ (H_a protons at 6.71 and 8.19 ppm; H_j protons at 6.87 and 7.53 ppm; H_k protons at 6.68 and 7.74 ppm,) provide clear evidence of the interchange of the "bound" and "free" status of the arms as discussed above. Also,

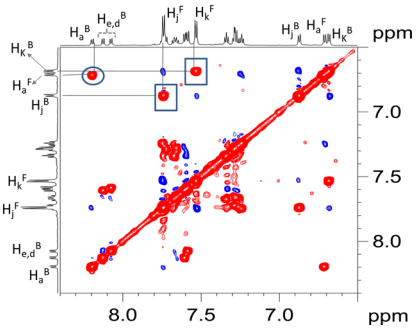

Figure 6. Partial ROESY spectrum of the $[\mathbf{1}\cdot\{\beta\text{-CD}\}]Cl_3$ complex at mole ratio 1:4 obtained on a 700 MHz spectrometer at 298 K. Exchange and NOE cross peaks are shown in red and blue, respectively. The exchange cross peak between the H_a protons of the "bound" and "free" arms are indicated by a circle, while those corresponding to H_k and H_j protons are indicated by squares.

temperature-dependent ROESY spectra show the expected decrease in intensity of the exchange cross peaks at lower temperatures due to the reduced exchange rate (Figure S23, Supporting Information).

Examples of exchange between free and bound guest (or host) molecules during host–guest inclusion complex formation are common.[17d,25] However, a dynamic process involving inclusion of only one of the three equivalent arms of the guest molecule within the β-CD cavity at a given time as represented in Scheme 1 is rather uncommon. Attempts were also made to measure the exchange rates and evaluate the thermodynamic parameters for this exchange process by variable mixing time NOESY experiments at different temperatures (Figure S24, Supporting Information). The exchange rates were evaluated by fitting the equations for cross peak build-up and diagonal peak decay to the experimental data (Figure 7). At 300 K, the exchange rate of the arms between the

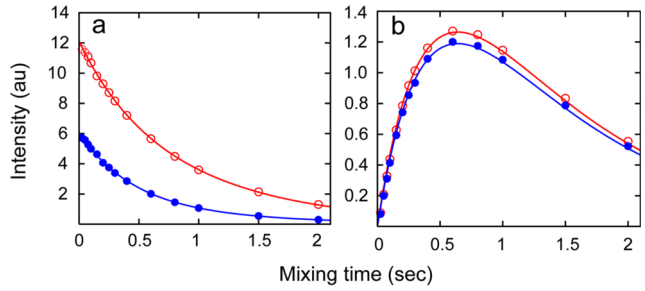

Figure 7. Fits of (a) decay and (b) build-up curves to experimental data for H_a protons of the naphthyl moiety (red: "free" arm and blue: "bound" arm) in $[\mathbf{1}\cdot\{\beta\text{-CD}\}]Cl_3$ at 300 K.

"free" and "bound" states was 1.32 s^{-1}. The thermodynamic parameters ($\Delta H \sim -13$ kJ and $\Delta S \sim -0.3$ kJK^{-1}) for the exchange process were evaluated using Eyring plots (Figure S25, Supporting Information).

ROESY experiments also provide insights into the relative spatial orientation of $\mathbf{1}Cl_3$ in the β-CD cavity through connectivities via negative NOE cross peaks (Figure S17, Supporting Information). The "intra-arm" NOE cross peaks between protons of $\mathbf{1}Cl_3$ help to distinguish the "bound" and "free" arms in $[\mathbf{1}\cdot\{\beta\text{-CD}\}]Cl_3$. For example, cross peaks between H_i and H_j protons help to assign the chemical shifts

DOI: 10.1021/acs.joc.5b02353
J. Org. Chem. 2016, 81, 512–521

in the "bound" (4.39 and 6.87 ppm) and "free" (4.01 and 7.74 ppm) arms.

The protons of the "bound" arm of $\mathbf{1}Cl_3$ show strong cross peaks to all β-CD protons except H_1, which is located outside the host cavity (Figure S17, Supporting Information). The protons H_j and H_k of the "bound" arm show NOE cross peaks to H_3 (3.51 ppm) and H_5 (3.28 ppm) of β-CD. In addition, H_j and H_k protons of the "free" arms show unexpected NOE cross peaks to H_5 (3.28 ppm) and H_6 (3.56, 3.50 ppm) protons of β-CD. This can only arise if the bound β-CD molecule penetrates the bound arm of $\mathbf{1}Cl_3$ in such a way that the phenyl rings from the "free" arms also come well within the NOE limits of 5 Å (Scheme 1). The NOE cross peaks between protons of β-CD and the arms of $\mathbf{1}Cl_3$ thus give an indication of the extent to which the host molecule engulfs the guest molecule. Previous reports on host–guest complexes of dansyl derivatives with β-CD suggest the possibility of the inclusion of the naphthyl moiety via the narrow rim of β-CD.[26] Inclusion complexes of β-CD with amine and secondary ammonium ion derivatives have been shown to be stabilized by hydrogen bonding between the primary −OH group at the rim and amino group of the guest molecule.[27] A similar situation involving weak H-bonding between the secondary −OH group at the rim and the lone pair of electrons of the amine moiety could help in stabilizing the $[\mathbf{1}\cdot\{\beta\text{-CD}\}]Cl_3$ complex since the wide rim of β-CD is sufficiently close to the nitrogen atom of the tertiary amine. Thus, the model of the 1:1 host–guest complex proposed on the basis of observations from ROESY and NOESY experiments, as indicated in Scheme 1, seems plausible.

Apart from chemical shifts, observed line widths of the ^{1}H NMR signals of $\mathbf{1}Cl_3$ do not differ significantly on increasing the $\mathbf{1}Cl_3$:β-CD molar ratio from 1:1 to 1:4. This further confirms that only one of the three arms of the $\mathbf{1}Cl_3$ is bound in the complex (Figure S26, Supporting Information). At mole ratios below 1:1, signals from uncomplexed $\mathbf{1}Cl_3$ also appear in the ^{1}H spectrum, and exchange cross peaks are observed between the protons of uncomplexed $\mathbf{1}Cl_3$ and corresponding protons present in the "bound" and "free" arms of the complex (Figure S27, Supporting Information). The uncomplexed $\mathbf{1}Cl_3$ is present transiently during the exchange involving complexation of the different arms. As the concentration of β-CD increases, these exchange peaks involving uncomplexed $\mathbf{1}Cl_3$ tend to become weaker. In a solution with $\mathbf{1}Cl_3$:β-CD mole ratio 1:4, the population of the uncomplexed guest molecules is much lower, with very short life times making it impossible to detect the corresponding cross peaks in the exchange experiments.

The above discussion clearly reveals that $\mathbf{1}Cl_3$ forms a 1:3 host–guest complex ($[\mathbf{1}\cdot3\{CB[7]\}]Cl_3$) with CB[7] and a dynamic 1:1 host–guest complex ($[\mathbf{1}\cdot\{\beta\text{-CD}\}]Cl_3$) with β-CD. The difference in the complexes formed by CB[7] and β-CD with $\mathbf{1}Cl_3$ may be ascribed to the basic structural difference of the two host molecules.The CB[7] molecule has a pumpkin shape with symmetric portals, while β-CD has a tub shape with different portal sizes. The pumpkin structure of CB[7] helps to stabilize the guest molecule by the combined effect of two types of interactions: (i) ion–dipole interactions between the positive charges on the guest molecule and the carbonyl oxygens and (ii) the hydrophobic interactions between the guest molecule and the host cavity. The hydrophobic part of $\mathbf{1}Cl_3$ (naphthyl moiety) which resides within the CB[7] cavity and the cationic part of the guest located near the rim of the host helps to achieve strong binding. On the other hand, β-CD is composed of glucopyranose subunits with two cavity portals differing in size and the nature of the hydroxyl groups. The hydroxyl groups encircling the cavity entrances of β-CD help to stabilize the guest molecule by hydrogen-bonding interactions with the hydrophilic part of $\mathbf{1}Cl_3$, while the hydrophobic interior of β-CD interacts with the hydrophobic part of the guest molecule. In the inclusion complex with β-CD, the wider rim of the host resides close to the phenyl rings of $\mathbf{1}Cl_3$, hence steric effects would hinder the simultaneous approach of three β-CD molecules along the arms of $\mathbf{1}Cl_3$.

Association Constant and Thermodynamic Parameters. The host–guest complex formation between $\mathbf{1}Cl_3$ and CB[7] or β-CD and associated changes in thermodynamic parameters were investigated in aqueous solution at 298 K by ITC measurements (Figure 8). ITC studies of the inclusion

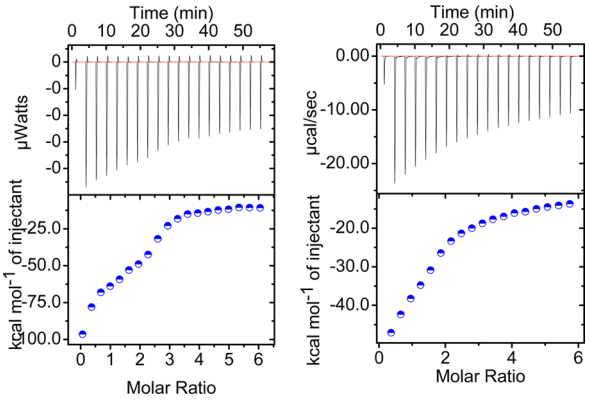

Figure 8. ITC profiles for the inclusion complex formation between (a) $\mathbf{1}Cl_3$ (0.116 mM) and CB[7] (3.42 mM) and (b) $\mathbf{1}Cl_3$ (0.116 mM) and β-CD (3.55 mM). Raw data for the sequential injection of the hosts into $\mathbf{1}Cl_3$ in steps of 2 μL are shown in the top panel. Heat evolution on addition of the hosts is shown in the bottom panel.

complex formation of $\mathbf{1}Cl_3$ with CB[7] and β-CD indicate binding stoichiometries of 1:3 and 1:1, respectively, which corroborates the results of NMR studies.

The binding constants for the sequential binding (data were fitted to a more than one site of binding sites model) of three CB[7] molecules to $\mathbf{1}Cl_3$ determined by ITC are $K_1 = (8.3 \pm 0.16) \times 10^3$ M^{-1}, $K_2 = (3.3 \pm 0.055) \times 10^4$ M^{-1}, and $K_3 = (1.5 \pm 0.021) \times 10^3$ M^{-1}, and the corresponding enthalpy changes are $\Delta H_1 = -2.44$, $\Delta H_2 = 1.09$, and $\Delta H_3 = -1.72$ kcal/mol. Inclusion complex formation also results in a large entropic loss ($T\Delta S_1 = -11.02$, $T\Delta S_2 = -7.92$, $T\Delta S_3 = -5.99$ kcal/mol). For host–guest complex formation between $\mathbf{1}Cl_3$ and β-CD, the fit for the one site binding model to the experimental data gives an association constant of $(1.44 \pm 0.7) \times 10^3$ M^{-1}. The inclusion complex formation is accompanied by a large entropy loss ($T\Delta S = -8.07$ kcal/mol) and a large negative enthalpy change ($\Delta H = -7.56 \pm 0.7$ kcal/mol). The large entropy loss observed in both cases during inclusion complex formation is probably due to the release of a large number of water molecules from the host cavities. The contribution of the desolvation effect to the entropy change is expected to be more prominent compared to the effects of reduced molecular flexibility of $\mathbf{1}Cl_3$ on complex formation. The binding constant for complex formation of $\mathbf{1}Cl_3$ with CB[7] is higher than that for β-CD. NMR studies show that in $[\mathbf{1}\cdot3\{CB[7]\}]Cl_3$, the three arms of $\mathbf{1}Cl_3$ are bound by the host resulting in a fairly rigid complex, while in $[\mathbf{1}\cdot\{\beta\text{-CD}\}]Cl_3$, the arms of $\mathbf{1}Cl_3$ exchange between

DOI: 10.1021/acs.joc.5b02353
J. Org. Chem. 2016, 81, 512–521

"bound" and "free" states, hence the complex is not highly rigid. Binding stoichiometry and binding affinity of $\mathbf{1}Cl_3$ toward CB[7] and β-CD determined by ITC agree well with the conclusions drawn from NMR studies.

Photophysical Studies. The UV–vis and steady-state emission spectra of $\mathbf{1}Cl_3$ were recorded in aqueous solution, and the spectral data are summarized in Table 1. The

Table 1. Photo Physical Data of $\mathbf{1}Cl_3$, $[\mathbf{1}\cdot 3\{CB\ [7]\}]Cl_3$ and $[\mathbf{1}\cdot\{\beta\text{-CD}\}]Cl_3$

host–guest complex	λ_{abs} (nm)	λ_{em} (nm)	Φ (%)	τ_{avg} (ns)[e]
$\mathbf{1}Cl_3$	309[a]	475[a]	1.1[a], 6.7[b]	0.3[d], 1.43[c]
$\{\mathbf{1}\cdot 3CB[7]\}\ Cl_3$	305[a]	388[a]	3.5[a]	0.80[d]
$\{\mathbf{1}\cdot\beta\text{-CD}\}\ Cl_3$	306[a]	475[a]	2.5[a]	2.63[c]

[a]Measurements in water. [b]Measurements in glycerol. [c]Monitoring the emission maximum at 475 nm. [d]Monitoring the emission maximum at 388 nm. [e]Average lifetime of the excited state obtained from TCSPC studies using a nano-LED as an excitation source (λ_{ext} = 295 nm) in water at 25 °C. For all measurements $1 \le \chi^2 \le 1.3$

absorption spectrum of $\mathbf{1}Cl_3$ in water shows an intense absorption band (ε = 2.3 × 10^5 L mol^{-1} cm^{-1}) with a maximum (λ_{max}) at 309 nm. The observed absorption band may be attributed to a π–π^* transition involving the triphenylamine and naphthyl moieties.

The solvatochromic behavior of $\mathbf{1}Cl_3$ was examined in different solvents with varying polarities. As the solvent polarity increases from hexane to water, a red shift of 18 nm is observed in the absorption spectrum (Figure S28, Supporting Information). On the other hand, the emission spectrum of $\mathbf{1}Cl_3$ (λ_{ext} of 309 nm) showed interesting changes with varying solvent polarities. In a nonpolar solvent such as hexane and others with low polarity indices (polarity index <5.2), the emission maximum occurs at 363 nm and remains practically unchanged, whereas in more polar solvents (polarity index >6.2), the emission maximum shifts linearly to longer wavelengths. The dependence of the emission maximum on polarity index of the solvent is indicated in Figure 9d.

In addition, a distinctly new emission spectral pattern arises as the solvent polarity increases (Figure S29, Supporting Information). For example, emission spectra of $\mathbf{1}Cl_3$ in DMF and water show entirely new broad emission maxima at 440 and 483 nm, respectively (Figure 9c). Earlier reports suggest that the naphthalene excimer fluorescence appears at ~425 nm.[28] In order to verify the possibility that the new emission band observed at 483 nm arises from the naphthalene excimer fluorescence, we obtained emission spectra of $\mathbf{1}Cl_3$ in water at concentrations ranging from 1.0–100.0 μM (Figure S30, Supporting Information). The lack of any significant enhancement in emission intensity at ~480 nm implies that naphthalene excimer fluorescence cannot account for the band observed at 483 nm. Thus, the band at 363 nm arises from a locally excited (LE) state, while the additional longer wavelength emission band observed in polar solvents (483 nm in water and 454 nm in DMSO; Figure S29, Supporting Information) arises from an ICT process.[29] Excitation spectra recorded by using λ_{ems} of 363 (in hexane) and 483 nm (in water) were distinctly different (Figure S31, Supporting Information). This implies that the emitting states associated with the 363 and 483 nm emission maxima are different. The LE state is stabilized in solvents with polarity indices ≤5.2, while the ICT state is stabilized in solvents with polarity indices ≥6.2. The quantum yields at λ_{ext} of 309 nm were determined for the two different emitting states of $\mathbf{1}Cl_3$ in two solvents of widely differing polarities; the observed quantum yield is 0.034 (Φ_{363}^{LE}) in hexane and 0.011 (Φ_{483}^{ICT}) in water. The decrease in the quantum yield with increase in solvent polarity has been described earlier for other analogous fluorophores.[30]

We also examined the effect of the addition of increasing amounts of CB[7] and β-CD on the absorption and emission spectra of $\mathbf{1}Cl_3$. On addition of 3 equiv of CB[7] or β-CD, the absorption spectrum of $\mathbf{1}Cl_3$ shows distinct hyperchromic shifts, however the band maximum remains the same (Figure S32, Supporting Information). On the other hand, significant differences in the emission spectral response are observed (Figure 9a,b). A decrease in the intensity of the emission band at 475 nm is observed on adding increasing amounts of CB[7] to an aqueous solution of $\mathbf{1}Cl_3$. Figure 9a shows that for $\mathbf{1}Cl_3$:CB[7] ≥ 0.12, a new emission band appears at 388 nm, but with no further shift of the emission maximum. As discussed above, emission bands at lower wavelengths arising from LE states are observed for $\mathbf{1}Cl_3$ in solvents with polarity indices ≤5.2. Literature reports have shown that the polarity of the cavity of CB[7] is similar to that of *n*-octanol (polarity index 3.2).[31] The disappearance of the emission band at 475 nm, and the subsequent appearance of a new emission band at 388 nm as the concentration of CB[7] increases, confirms the inclusion of $\mathbf{1}Cl_3$ in the CB[7] cavity which has a polarity index similar to that of a nonpolar solvent like *n*-octane thus leading to a LE state-based emission. The greater rigidity of $\mathbf{1}Cl_3$ on

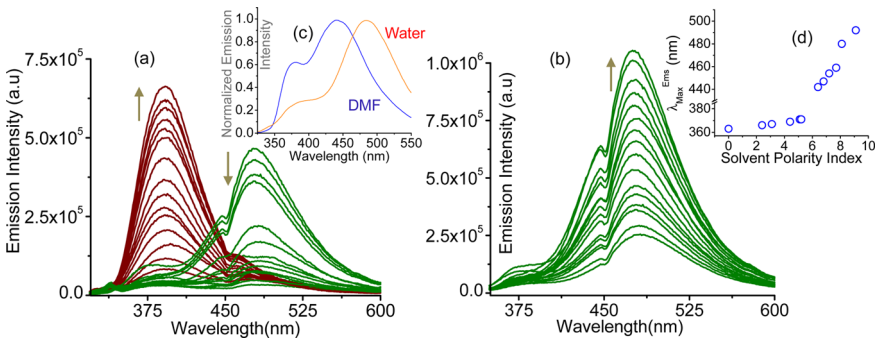

Figure 9. Changes in luminescence spectral pattern of $\mathbf{1}Cl_3$ on addition of increasing amounts of (a) CB[7] = 0–17.25 × 10^{-5} M and (b) β-CD = 0–8.3 × 10^{-5} M. The $\mathbf{1}Cl_3$ concentrations are 2.08 × 10^{-5} M and 1.05 × 10^{-5} M. (c) Normalized emission spectra of $\mathbf{1}Cl_3$ in water and DMF depicting the dual emission bands. (d) Plot of λ_{ems}^{max} for $\mathbf{1}Cl_3$ in solvents with different polarity indices. λ_{ext} of 309 nm was used for all measurements.

DOI: 10.1021/acs.joc.5b02353
J. Org. Chem. 2016, 81, 512–521

forming the 1:3 host–guest complex ($[\mathbf{1}\cdot 3\{CB[7]\}]Cl_3$) also favors the nonradiative pathway for the deactivation of the excited state and accounts for the increased quantum yield (Φ = 0.035) for the emission band at 388 nm compared to $\mathbf{1}Cl_3$ (Table 1).

In contrast, the emission responses of $\mathbf{1}Cl_3$ on addition of increasing amounts of β-CD are significantly different. The intensity of the emission band at 475 nm is enhanced considerably with increasing concentration of β-CD (Figure 9b). The polarity index of the cavity of β-CD is much higher and is expected to favor an ICT process.[32] The emission quantum yield (Φ = 0.025) in the complex with β-CD is also higher compared to free $\mathbf{1}Cl_3$ (Table 1). Inclusion of even one of the three arms of $\mathbf{1}Cl_3$ by β-CD imposes sufficient rigidity in $\mathbf{1}Cl_3$ as compared to free $\mathbf{1}Cl_3$. This could account for the increased emission quantum yield in the β-CD complex compared to free $\mathbf{1}Cl_3$ and the favoring of the radiative deactivation of the excited state. In order to explore this possibility further, we examined the emission behavior of $\mathbf{1}Cl_3$ in glycerol, a solvent with high polarity (polarity index 6.45) and viscosity. The high solvent viscosity is expected to decrease the molecular flexibility of $\mathbf{1}Cl_3$ significantly along with the associated nonradiative deactivation. A substantial increase in emission quantum yield (Φ = 0.067) for the ICT-based emission band is observed at 473 nm in glycerol when compared to that in water which is less viscous (Table 1).

Luminescence decay profiles following excitation at 295 nm were obtained for the excited state of $\mathbf{1}Cl_3$ in the free state and in the complexes with CB[7] and β-CD (Figure S33, Supporting Information) by using time-correlated single photon counting (TCSPC) technique. The decay time constants are included in Table 1. Both, the ICT-based excited state monitored at 475 nm and the LE state monitored at 388 nm show multicomponent emission decays. This is probably due to the presence of an equilibrium between different conformers in solution having slightly different emission decay time constants. In the free state, $\mathbf{1}Cl_3$ shows average excited-state lifetimes of 0.3 ($\tau_{avg}^{388\text{-LE}}$) and 1.43 ns ($\tau_{avg}^{475\text{-ICT}}$) at 388 and 475 nm, respectively. In the complex with CB[7] ($[\mathbf{1}\cdot 3\{CB[7]\}]Cl_3$), the LE state at 388 nm shows $\tau_{avg}^{388\text{-LE}}$ of 0.8 ns, which is higher than that observed in the free state of $\mathbf{1}Cl_3$. On complexation with β-CD ($[\mathbf{1}\cdot\{\beta\text{-CD}\}]Cl_3$), $\tau_{avg}^{475\text{-ICT}}$ of the ICT-based excited state at 475 nm is enhanced to 2.63 ns. At 475 nm, the photon counts were too low for the $[\mathbf{1}\cdot 3\{CB[7]\}]Cl_3$ complex, hence reliable measurements were not possible. Similarly photon counts were low for ($[\mathbf{1}\cdot\{\beta\text{-CD}\}]Cl_3$) at 388 nm. The formation of a 1:3 host–guest complex with CB[7] enhances the lifetime of the LE state, while the 1:1 host–guest complex formation with β-CD enhances the lifetime of the ICT state with respect to that of free $\mathbf{1}Cl_3$ along with corresponding increase in the emission quantum yield, Φ. This is in accordance with earlier reports of increase in quantum yield on inclusion complex formation.[21,33,34]

The steady-state emission studies clearly show that through appropriate choice of the host molecules (for example, CB[7] or β-CD), it is possible to stabilize two completely different excited states in a TPA derivative in solution phase at room temperature following excitation at a particular wavelength. With CB[7], a 1:3 host–guest complex formation helps in stabilizing the LE state of $\mathbf{1}Cl_3$ with an emission maximum at 388 nm, whereas a 1:1 host–guest complex formation with β-CD helps in stabilizing the ICT state of $\mathbf{1}Cl_3$ with emission maximum at 475 nm. In the $[\mathbf{1}\cdot 3\{CB[7]\}]Cl_3$ complex, all the three arms of $\mathbf{1}Cl_3$ are trapped within host cavities of relatively low polarity, while in the $[\mathbf{1}\cdot\{\beta\text{-CD}\}]Cl_3$ complex, a single arm of $\mathbf{1}Cl_3$ is trapped at any given time within a host cavity of higher polarity. Thus, the differences in the mobility of $\mathbf{1}Cl_3$ on complex formation with the two different host molecules having cavities of differing polarities account for the different emission behavior observed in the two cases.

CONCLUSION

We synthesized a new TPA derivative ($\mathbf{1}Cl_3$), which exhibits a rare dual emission property in solution at room temperature. The shorter wavelength emission band arises from a locally excited state, while the longer wavelength emission band results from an ICT process. Observation of dual emission from a single molecule at room temperature is rather uncommon. In presence of CB[7] and β-CD, the $\mathbf{1}Cl_3$ molecule forms inclusion complexes that are significantly different. NMR studies show that a 1:3 host–guest complex is formed on complexation with CB[7] ($[\mathbf{1}\cdot 3\{CB[7]\}]Cl_3$), while a 1:1 host–guest complex is formed with β-CD ($[\mathbf{1}\cdot\{\beta\text{-CD}\}]Cl_3$). The latter exists in a dynamic equilibrium in which only one of the three arms of $\mathbf{1}Cl_3$ is bound to a β-CD molecule at a given time. The two complexes also show very different emission behavior, with $[\mathbf{1}\cdot 3\{CB[7]\}]Cl_3$ favoring emission from a locally excited state and $[\mathbf{1}\cdot\{\beta\text{-CD}\}]Cl_3$ favoring an ICT-based excited state. The difference in the nature of complex formation and emission behavior of $\mathbf{1}Cl_3$ with the two host molecules was examined in detail by NMR, electronic, and steady-state fluorescence spectroscopic techniques. The differing shapes, electrostatic surface potentials of the host molecules, and the differences in polarities of the two host cavities[35] account for the very different emission responses in the two cases.

EXPERIMENTAL SECTION

Chemicals. 1-Naphthylmethylamine and tris(*para*-formylphenyl) amine were purchased and used without further purification. All the solvents were purchased and used after purification according to standard procedures.

Synthesis of $\mathbf{1}Cl_3$. 1-Naphthylmethylamine (0.382g, 0.607 mM) was added to tris(*para*-formyl phenyl) amine (0.2 g, 0.243 mM) and dissolved in 30 mL of dry acetonitrile/methanol mixture with volume ratio 1:1. The reaction mixture was stirred at room temperature for 24 h, and the solvent mixture was evaporated under reduced pressure. Methanol was added to the reaction mixture, and the temperature was reduced to 0 °C. $NaBH_4$ (0.6 g) was then added in portions to the cooled reaction mixture. The reaction mixture was allowed to reach room temperature and stirred for 6 h. The solvent was removed under reduced pressure, and the residue was extracted three times with DCM (30 mL) and water. The organic layers were combined and dried with anhydrous sodium sulfate. The solvent was removed under reduced pressure to collect the crude product, which was purified on a silica gel column using chloroform/methanol (98:2, by volume) as an eluent. The desired product was obtained as a yellow sticky solid. A solution of concentrated HCl (0.2 mL) in methanol was added dropwise and stirred for 24 h. A yellow solid was formed (336 mg, 64%), which was isolated as a precipitate, collected by filtration, and dried over P_2O_5. ^{1}H NMR (500 MHz, CD_3OD, ppm): 8.00–8.04 (10H, m), 7.72 (3H, d, 7 Hz), 7.57–7.68 (11H, m), 7.54 (6H, d, J = 8.5 Hz), 7.20 (6H, d, J = 8.5 Hz), 4.77 (6H, s), 4.40 (6H, s). ^{13}C NMR (500 MHz, DMSO-d_6, ppm): 147.6, 133.7, 132.3, 131.5, 129.9, 129.4, 129.1, 127.1, 126.7, 125.8, 124.1, 123.9, 50.4, 46.8. Elemental analysis: Calculated for $C_{54}H_{51}N_4Cl_3$: C, 75.21; H, 5.96; N, 6.50. Found: C, 74.93; H, 5.99; N, 6.46. ESI-MS: Calculated: 395.16; observed: 395.21 $[M - 2Cl^-]^{2+}/2$; melting point 190–195 °C.

DOI: 10.1021/acs.joc.5b02353
J. Org. Chem. 2016, 81, 512–521

NMR Spectroscopy. NMR experiments were carried out on 700 and 500 MHz spectrometers. Samples were prepared in D_2O, and spectra were obtained at 298 K unless stated otherwise. Proton NMR titration measurements were carried out by adding increasing amounts of hosts CB[7] or β-CD to a 1.5 mM solution of $\mathbf{1}Cl_3$. In the case of complex formation with CB[7], the variation in the chemical shift of the H_i proton was monitored in the titration experiments. The extent of complexation, $p = \Delta/\Delta_0$ was estimated from a plot of $\Delta = \delta_c - \delta_u$ vs $1/[CB7]$, where δ_c and δ_u are the H_i chemical shifts in the presence and absence of CB[7], respectively, and Δ_0 = 0.2358 (Figure S8, Supporting Information).

Homodecoupled pure shift spectra were recorded as described.[24] Pure shift time domain data were constructed from 32 "chunks" of free induction decay measured for 20 ms each. Refocusing of scalar couplings was accomplished by low flip angle CHIRP pulses in combination with a hard 180° pulse. Homonuclear 2D NMR experiments were performed with 256 × 2 K data points, employing a relaxation delay of 2 s. Heteronuclear 2D NMR experiments were recorded with 140 × 1 K or 256 × 1 K data points. Data were acquired in Echo-Antiecho or States-TPPI mode, except for the COSY experiment which was recorded in magnitude mode. Typically, mixing times of 80 ms, 250 ms, and 1s were employed for TOCSY, ROESY and NOESY experiments, respectively.

Isothermal Titration Calorimetry. Isothermal titration calorimetric (ITC) measurements were carried out by mixing solutions at 1000 rpm stirring. The complex formation between $\mathbf{1}Cl_3$ and the hosts CB[7] and β-CD was monitored in aqueous solution at 25 °C. About 200 μL of the host solution was titrated against a solution of $\mathbf{1}Cl_3$. A typical titration experiment consisted of 19 consecutive injections of 2 μL of the host at 20 s duration each with a 180 s interval between injections. Heat of dilution of the guest was determined by injecting $\mathbf{1}Cl_3$ solution into the neat solvent, and the observed heats of binding were corrected for the heat of dilution. The data were analyzed to determine the binding constant (K), binding stoichiometry (N), change of enthalpy (ΔH), and the change of entropy (ΔS) associated with complex formation between $\mathbf{1}Cl_3$ and the two host molecules.

Optical Spectroscopy. The absorption and emission spectra were recorded on UV−vis-NIR spectrometer and luminescence spectrofluorimeter at 25 °C. All absorption and emission spectra measurements were performed with freshly prepared solutions, and appropriate background corrections were applied. Fluorescence lifetimes were measured by TCSPC using a luminescence spectrofluorimeter. A nano-LED was used as the excitation source (λ_{ext} = 295 nm). Fluorescence quantum yield (Φ_f) was determined using quinine hemisulfate as a reference by employing the following equation:

$$\Phi_S = \Phi_R \frac{A_S}{A_R} \times \frac{(Abs)_R}{(Abs)_S} \times \frac{\eta_S^2}{\eta_R^2}$$

where A_i is the integrated area under the fluorescence curve, Abs_i denotes the absorption, η_i is the refractive index of the medium, and Φ_i is the fluorescence quantum yield. The subscripts i = S, R refers to the parameters corresponding to the sample and reference compound, respectively.

■ ASSOCIATED CONTENT

Supporting Information

The Supporting Information is available free of charge on the ACS Publications website at DOI: 10.1021/acs.joc.5b02353.

Spectral characterization data for $\mathbf{1}Cl_3$, ^{1}H NMR titration spectra, ^{13}C spectra, 2D NMR spectra and mass spectra for complexes ($[\mathbf{1}\cdot 3\{CB[7]\}]Cl_3$) and ($[\mathbf{1}\cdot\{\beta\text{-CD}\}]Cl_3$), variable-temperature NMR spectra and 2D exchange spectroscopy data analysis for ($[\mathbf{1}\cdot\{\beta\text{-CD}\}]Cl_3$), absorption and emission spectral data for $\mathbf{1}Cl_3$ and the complexes ($[\mathbf{1}\cdot 3\{CB[7]\}]Cl_3$) and ($[\mathbf{1}\cdot\{\beta\text{-CD}\}]Cl_3$) (PDF)

■ AUTHOR INFORMATION

Corresponding Authors

*E-mail: pr.rajamohanan@ncl.res.in.

*E-mail: a.das@ncl.res.in.

Notes

The authors declare no competing financial interest.

■ ACKNOWLEDGMENTS

The authors thank Mr. Tuhin Khan from Indian Institute of Technology, Mumbai for help with the TCSPC studies. M.G. acknowledges Council of Scientific and Industrial Research (CSIR), India for research fellowships. A.D. thanks Science and Engineering Research Council (SERC grant no. SB/S1/IC-23/2013), Department of Science and Technology (DST), India and CSIR-NCL (grant no. MLP 028226) for financial support. The Authors acknowledge CSIR, for research grants under the 12th five year plan project (grant no. CSC 0405).

■ REFERENCES

(1) (a) Yasuda, Y.; Kamiyama, T.; Shirota, Y. *Electrochim. Acta* **2000**, *45*, 1537−1548. (b) Ostrauskaite, J.; Voska, V.; Antulis, J.; Gaidelis, V.; Jankauskas, V.; Grazulevicius, J. V. *J. Mater. Chem.* **2002**, *12*, 3469−3474. (c) Zhao, L.; Lin, Y.; Liu, T.; Li, H.; Xiong, Y.; Yuan, W. Z.; Sung, H. H.-Y.; Williams, I. D.; Zhang, Y.; Tang, B. Z. *J. Mater. Chem. C* **2015**, *3*, 4903−4909.

(2) (a) Chandra, B. P. *Indian J. Pure Appl. Phys.* **1980**, *18*, 743−746. (b) Yum, J.-H.; Moser, J.-E.; Yi, C.; Nazeeruddin, M. K.; Grätzel, M. *Nat. Commun.* **2012**, *3*, 631. (c) Wu, J.-H.; Liou, G.-S. *Adv. Funct. Mater.* **2014**, *24*, 6422−6429.

(3) (a) Beaupré, S.; Dumas, J.; Leclerc, M. *Chem. Mater.* **2006**, *18*, 4011−4018. (b) Shirota, Y.; Kageyama, H. *Chem. Rev.* **2007**, *107*, 953−1010. (c) Field, J. E.; Muller, G.; Riehl, J. P.; Venkataraman, D. *J. Am. Chem. Soc.* **2003**, *125*, 11808−10809. (d) Friend, R. H.; Gymer, R. W.; Holmes, A. B.; Burroughes, J. H.; Marks, R. N.; Taliani, C.; Bradley, D. D. C.; Dos Santos, D. A.; BreÂ das, J. L.; gdlund LoÈ, M.; Salaneck, W. R. *Nature* **1999**, *397*, 121−128.

(4) (a) Wei, P.; Bi, X. D.; Wu, Z.; Xu, Z. *Org. Lett.* **2005**, *7*, 3199−3202. (b) Fang, Z.; Teo, T. L.; Cai, L.; Lai, Y. H.; Samoc, A.; Samoc, M. *Org. Lett.* **2009**, *11*, 1−4.

(5) (a) Lueck, H. B.; McHale, J. L.; Edwards, W. D. *J. Am. Chem. Soc.* **1992**, *114*, 2342−2348. (b) Meijer, G.; Berden, G.; Meerts, W. L.; Hunziker, H. E.; de Vries, M. S.; Wendt, H. R. *Chem. Phys.* **1992**, *163*, 209−222.

(6) (a) Malagoli, M.; Bredas, J. L. *Chem. Phys. Lett.* **2000**, *327*, 13−17. (b) Reva, I.; Lapinski, L.; Chattopadhyay, N.; Fausto, R. *Phys. Chem. Chem. Phys.* **2003**, *5*, 3844−3850.

(7) Ranasinghe, M. I.; Varnavski, O. P.; Pawlas, J.; Hauck, S. L.; Louie, J.; Hartwig, J. F.; Goodson, T. *J. Am. Chem. Soc.* **2002**, *124*, 6520−6521.

(8) (a) Kobayashi, H.; Hama, Y.; Koyama, Y.; Barett, T.; Regino, C. A. S.; Celeste, A.; Urano, Y. *Nano Lett.* **2007**, *7*, 1711−1716. (b) Wang, L.; Zhao, W. J.; O' Donoghue, M. B.; Tan, W. H. *Bioconjugate Chem.* **2007**, *18*, 297−301.

(9) (a) Browne, K. A.; Deheyn, D. D.; Brown, R. C.; Weeks, I. *Anal. Chem.* **2012**, *84*, 9222−9229. (b) Wang, L.; Tan, W. *Nano Lett.* **2006**, *6*, 84−88.

(10) (a) Nathani, R. I.; Moody, P.; Chudasama, V.; Smith, M. E. B.; Fitzmaurice, R. J.; Caddick, S. *Chem. Sci.* **2013**, *4*, 3455−3458. (b) Rashidian, M.; Kumarapperuma, S. C.; Gabrielse, K.; Fegan, A.; Wagner, C. R.; Distefano, M. D. *J. Am. Chem. Soc.* **2013**, *135*, 16388−16396.

(11) (a) Xu, J.; Ma, L.; Guo, P.; Zhuang, X.; Zhu, X.; Hu, W.; Duan, X.; Pan, A. *J. Am. Chem. Soc.* **2012**, *134*, 12394−12937. (b) Huang, J.; Sun, N.; Dong, Y.; Tang, R.; Lu, P.; Cai, P.; Li, Q.; Ma, D.; Qin, J.; Li, Z. *Adv. Funct. Mater.* **2013**, *23*, 2329−2337. (c) Yao, L.; Zhang, S.;

DOI: 10.1021/acs.joc.5b02353
J. Org. Chem. 2016, 81, 512−521

Wang, R.; Li, W.; Shen, F.; Yang, B.; Ma, Y. *Angew. Chem.* **2014**, *126*, 2151−2155.
(12) (a) Muller, C. D.; Falcou, A.; Reckefuss, N.; Rojahn, M.; Widerhirn, V.; Rudati, P.; Frohne, H.; Nuyken, O.; Becker, H.; Meerholz, K. *Nature* **2003**, *421*, 829−833. (b) Zhao, Y. S.; Fu, H. B.; Hu, F. Q.; Peng, A. D.; Yao, J. N. *Adv. Mater.* **2007**, *19*, 3554−3558. (c) Lei, T.; Cao, Y.; Fan, Y.; Liu, C.-J.; Yuan, S.-C.; Pei, J. *J. Am. Chem. Soc.* **2011**, *133*, 6099−6101.
(13) (a) Blakley, R. L.; DeArmond, M. K. *J. Am. Chem. Soc.* **1987**, *109*, 4895−4901. (b) Suzuki, T.; Kuchiyama, T.; Kishi, S.; Kaizaki, S.; Takagi, H. D.; Kato, M. *Inorg. Chem.* **2003**, *42*, 785−795.
(14) (a) Zhu, C.-N.; Jiang, P.; Zhang, Z.-L.; Zhu, D.-L.; Tian, Z.-Q.; Pang, D.-W. *ACS Appl. Mater. Interfaces* **2013**, *5*, 1186−1193. (b) Anikeeva, P. O.; Halpert, J. E.; Bawendi, M. G.; Bulović, V. *Nano Lett.* **2009**, *9*, 2532−2536. (c) Wang, C.; Xu, S.; Shao, Y.; Wang, Z.; Cui, Q.; Y, X. *J. Mater. Chem. C* **2014**, *2*, 5111−5115.
(15) (a) Keyes, T. E.; O'Connor, C.; Vos, J. G. *Chem. Commun.* **1998**, 889−890. (b) Glazer, E. C.; Magde, D.; Tor, Y. *J. Am. Chem. Soc.* **2005**, *127*, 4190−4192.
(16) (a) Honda, K.; Fujishima, S. h; Ojida, A.; Hamachi, I. *ChemBioChem* **2007**, *8*, 1370−1372. (b) Chen, Q.; Zhang, X.; Sun, Y.; Ritt, M.; Sivaramakrishnan, S.; Fan, X. *Lab Chip* **2013**, *13*, 2679−2681.
(17) (a) Mandal, A. K.; Gangopadhyay, M.; Das, A. *Chem. Soc. Rev.* **2015**, *44*, 663−676. (b) Wang, R.; Yuan, L.; Macartney, D. H. *Chem. Commun.* **2005**, 5867−5869. (c) Pischel, U.; Uzunova, V. D.; Remon, P.; Nau, W. M. *Chem. Commun.* **2010**, *46*, 2635−2637. (d) Shukla, A. D.; Bajaj, H. C.; Das, A. *Angew. Chem., Int. Ed.* **2001**, *40*, 446−448.
(18) (a) He, Z.; Jiang, W.; Schalley, C. A. *Chem. Soc. Rev.* **2015**, *44*, 779−789. (b) Wei, P.; Yan, X.; Huang, F. *Chem. Soc. Rev.* **2015**, *44*, 815−832. (c) Cheng, H.-B.; Zhang, H.-Y.; Liu, Y. *J. Am. Chem. Soc.* **2013**, *135*, 10190−10193. (d) Jie, K.; Zhou, Y.; Yao, Y.; Huang, F. *Chem. Soc. Rev.* **2015**, *44*, 3568−3587.
(19) (a) Yan, Y.; Tao, X.; Sun, Y.; Xu, G.; Wang, C.; Yang, J.; Zhao, X.; Wu, Y.; Ren, Y.; Jiang, M. *Mater. Chem. Phys.* **2005**, *90*, 139−143. (b) Zheng, B.; Klautzsch, F.; Xue, M.; Huang, F.; Schalley, C. A. *Org. Chem. Front.* **2014**, *1*, 532−540. (c) Cera, L.; Schalley, C. A. *Chem. Sci.* **2014**, *5*, 2560−2567.
(20) (a) Lee, H. J.; Sohn, J.; Hwang, J.; Park, S. Y. *Chem. Mater.* **2004**, *16*, 456−465. (b) Lartia, R.; Allain, C.; Bordeau, G.; Schmidt, F.; Fiorini-Debuisschert, C.; Charra, F.; Teulade-Fichou, M.-P. *J. Org. Chem.* **2008**, *73*, 1732−1744.
(21) Mandal, A. K.; Suresh, M.; Das, P.; Das, A. *Chem. - Eur. J.* **2012**, *18*, 3906−3917.
(22) Sindelar, V.; Moon, K.; Kaifer, A. E. *Org. Lett.* **2004**, *6*, 2665−2668.
(23) (a) Perlmutter-Hayman, B. *Acc. Chem. Res.* **1986**, *19*, 90−96. (b) Gibson, H. W.; Yamaguchi, N.; Hamilton, L.; Jones, J. W. *J. Am. Chem. Soc.* **2002**, *124*, 4653−4665. (c) Huang, F.; Jones, J. W.; Gibson, H. W. *J. Org. Chem.* **2007**, *72*, 6573−6576.
(24) Foroozandeh, M.; Adams, R. W.; Meharry, N. J.; Jeannerat, D.; Nilsson, M.; Morris, G. A. *Angew. Chem., Int. Ed.* **2014**, *53*, 6990−6992.
(25) (a) Ashton, P. R.; Baxter, I.; Fyfe, M. C. T.; Raymo, F. M.; Spencer, N.; Stoddart, J. F.; White, A. J. P.; Williams, D. J. *J. Am. Chem. Soc.* **1998**, *120*, 2297−2307. (b) Affeld, A.; Hübner, G. M.; Seel, C.; Schalley, C. A. *Eur. J. Org. Chem.* **2001**, *2001*, 2877−2890.
(26) (a) Nakashima, H.; Yoshida, N. *Org. Lett.* **2006**, *8*, 4997−5000. (b) Corradini, R.; Dossena, A.; Marchelli, R.; Panagia, A.; Sartor, G.; Saviano, M.; Lombardi, A.; Pavone, V. *Chem. - Eur. J.* **1996**, *2*, 373−381. (c) Corradini, R.; Dossena, A.; Galaverna, G.; Marchelli, R.; Panagia, A.; Sartor, G. *J. Org. Chem.* **1997**, *62*, 6283−6289.
(27) (a) Rao, T. V. S. D.; Lawrence, S. *J. Am. Chem. Soc.* **1990**, *112*, 3614−3615. (b) Catena, G. C.; Bright, F. V. *Anal. Chem.* **1989**, *61*, 905−909. (c) Isnin, R.; Kaifer, A. E. *J. Am. Chem. Soc.* **1991**, *113*, 8188−8190. (d) Nepal, D.; Samal, S.; Geckeler, K. E. *Macromolecules* **2003**, *36*, 3800−3802.
(28) Chandross, E. A.; Dempster, C. J. *J. Am. Chem. Soc.* **1970**, *92*, 704−706.
(29) (a) Diwu, Z.; Zhang, C.; Klaubert, R. P.; Haughland, J. *J. Photochem. Photobiol., A* **2000**, *131*, 95−97. (b) Detert, H.; Schmidt, V. *J. Phys. Org. Chem.* **2004**, *17*, 1051−1056.
(30) Woo, H. Y.; Liu, B.; Kohler, B.; Korystov, D.; Mikhailovsky, A.; Bazan, G. C. *J. Am. Chem. Soc.* **2005**, *127*, 14721−14729.
(31) Nau, W. M.; Florea, M.; Assaf, K. I. *Isr. J. Chem.* **2011**, *51*, 559−577.
(32) (a) Cox, G. S.; Turro, N. J. *J. Am. Chem. Soc.* **1984**, *106*, 422−424. (b) Heredia, A.; Requena, G.; Sanchez, F. G. *J. Chem. Soc., Chem. Commun.* **1985**, 1814−1815.
(33) (a) Oster, G.; Nishijima, Y. *J. Am. Chem. Soc.* **1956**, *78*, 1581−1584. (b) Wagner, B. D.; Stojanovic, N.; Day, A. I.; Blanch, R. J. *J. Phys. Chem. B* **2003**, *107*, 10741−10746.
(34) Berezin, M. Y.; Achilefu, S. *Chem. Rev.* **2010**, *110*, 2641−2684.
(35) (a) Dsouza, R. N.; Pischel, U.; Nau, W. M. *Chem. Rev.* **2011**, *111*, 7941−7980. (b) Kim, K.; Selvapalam, N.; Ko, Y. H.; Park, K. M.; Kim, D.; Kim, J. *Chem. Soc. Rev.* **2007**, *36*, 267−279. (c) Bhasikuttan, A. C.; Pal, H.; Mohanty, J. *Chem. Commun.* **2011**, *47*, 9959−9971.

DOI: 10.1021/acs.joc.5b02353
J. Org. Chem. 2016, 81, 512−521